

Ultimate Strength Evaluation of Kuroshio Current Turbine Blades

Chi-Fang Lee*, Chien-Ting Sun*, Ching-Yeh Hsin**, Ya-Jung Lee*, Forng-Chen Chiu***, Tsung-Yueh Lin*

*Research Department, CR Classification Society, Taipei, Taiwan

**Systems Engineering and Naval Architecture Department, National Taiwan Ocean University, Keelung, Taiwan

***Engineering Science and Ocean Engineering Department, National Taiwan University, Taipei, Taiwan

ABSTRACT

This study focuses on the ultimate strength assessment of the Fiber-Reinforced Plastic (FRP) sandwich-structured composite blades of a current turbine under normal and abnormal conditions. The structural response was evaluated through finite element analyses that reproduced the interaction between the core and the FRP layers. This study discusses the design extreme loads assessment, the finite element modeling of the blades, and the related strength criteria to be considered.

KEY WORDS: Current Turbine; FRP Blade; Ultimate Strength; Root Connection.

INTRODUCTION

The Kuroshio Current flows along the east coast of Taiwan from the Philippines to Japan following a northeast direction. The Kuroshio Current being relatively steady in amplitude and in direction, not much affected by tides, and, with an average velocity of 1.5 m/s, could offer an economically viable source of energy to Taiwan. However, numerous marine creatures live and travel in the Kuroshio Current for its warm temperature and high velocity, which increases the probability of collisions with immersed current turbines. Therefore, a research project funded by Taiwan's Ministry of Science and Technology was conducted by National Taiwan University (NTU) and National Taiwan Ocean University (NTOU) to evaluate the feasibility of a 0.5 MW Floating Kuroshio Current Turbine (FKT).

This study focuses on the ultimate strength assessment of the Fiber-Reinforced Plastic (FRP) sandwich-structured composite blades, including the root connection under normal and abnormal conditions. The extreme loads arising during nominal power production were produced by RANS-formulation CFD simulations (Chiu, Lai, Lee, Tzeng, and Hsin, 2018), and the structural strength of the blades and root connections was verified against yielding as per the rules (DNVGL, 2015, BV, 2015). Besides, the accidental loads arising from collision were considered in a 'fail safe' manner, where quasi-static concentrated forces were applied at the blade tip with increasing amplitudes until the failure of the blade, while the strength of the root connection made of

steel parts was verified against yielding. This design approach enabled us to ensure that the failure of the blades will occur before compromising the structural integrity of the blade root connection, thereby limiting the cost of blade replacement operations.

FKT MODEL DESCRIPTION

The Floating Kuroshio Turbine (FKT) is a horizontal axis hydroturbine designed to convert the kinetic energy of the Kuroshio Current into electrical energy. Fig. 1 shows an overview of the fully-immersed current turbine generator with its mooring system (Chiu, Lin, and Lin, 2015). The FKT consists of two nacelle-rotor assemblies that are supported by vertical beams at each end of a horizontal foil-float and transversally connected by a cross-beam, as shown in Fig. 2.

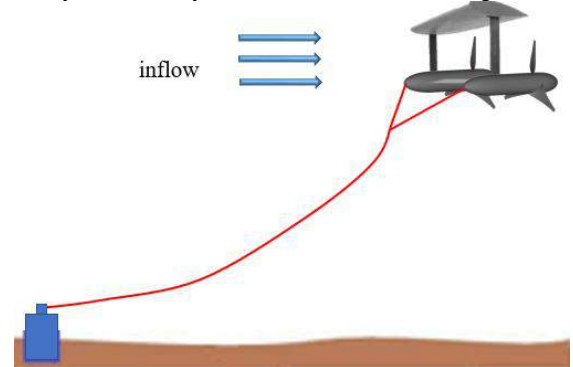


Fig. 1 General overview of the 0.5 MW Floating Kuroshio Turbine and its mooring system.

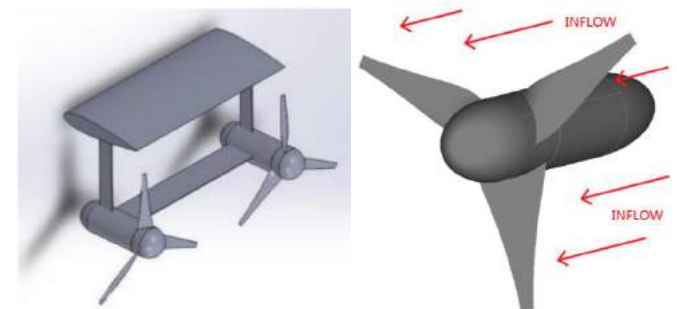


Fig. 2 Detailed views of the 0.5 MW Floating Kuroshio Turbine floater

and nacelle-rotor assemblies.

The FKT is designed to operate at an immersed depth of 50 m. The rotors consist of 3 blades of 5.0 m tip-diameter, and the nacelle is capped by a spinner of 1.2 m diameter.

BLADE STRUCTURE

The blades are FRP sandwich-structured composite parts that consist of two stiff FRP skins (pressure and suction side) attached to a lightweight core material, as shown in Fig. 3. This design enables reducing the weight of the blades while ensuring sufficient strength and stiffness. The FRP skins are made of 29 plies of epoxy resin reinforced with glass-fiber of various orientations, for which the main orientation, here 0° , is set along the blade length.

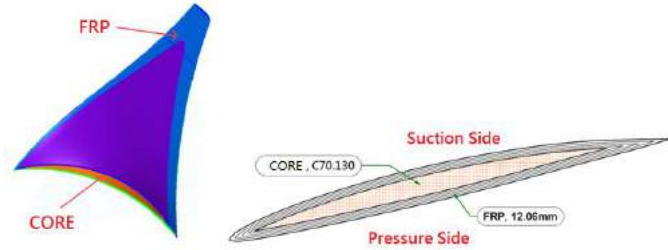


Fig. 3 FRP sandwich structure of the blade.

The FRP layers are made of Quadriaxial (DBLT1800) fabrics (0° , $+45^\circ$, 90° , -45°), chopped strand mat (M225) fabrics, and Uniaxial (L900) fabrics (0°). Fig. 4 shows the laminate arrangement of one FRP skin. Eventually, the FRP skins are approximately 12.05 mm thick. Table 1 lists the material properties of FRP laminates (i.e. fiber/resin mix). The foam core is represented through an isotropic material with a Young's modulus of 95 MPa and minimum tensile strength of 3 MPa.

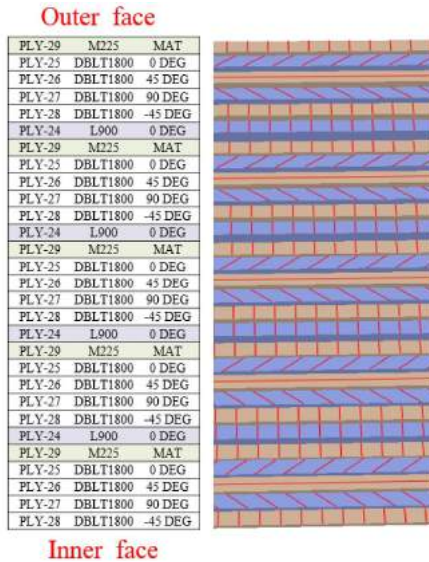


Fig. 4. Definition of the Lay-up of one FRP skin.

Table 1. Material properties of the FRP laminates.

	DBLT1800	M225	L900	(Unit)
E	34354/7647	14723	36617/8359	MPa
G	2867/2007	5663/1696	3082/2157	MPa
ν	0.285	0.3	0.281	-

σ_1	494.7(T)	182.6(T)	790.9(T)	MPa
	/445.2(C)	/164.3(C)	/711.8(C)	
σ_2	110.1(T)	182.6(T)	28.1(T)	MPa
	/99.1(C)	/164.3(C)	/25.29(C)	

Note:

E= Young's modulus

G= Shear modulus

ν = Poisson ratio

σ_i = Tensile strength for i direction of fibers

BLADE-ROOT CONNECTION

The blade root is connected to the rotor shaft through a bolted bracket assembly (see Fig. 5). The bracket is made of a stainless steel U-profile, and a stainless steel spacer is inserted between the FRP skins to transmit through the blade-root the compression loads generated by the preload of eight M20 bolts, as shown in Fig. 6. The U-bracket is bolted to the rotor shaft that is flattened in way of each blade root. Finally a spinner shell is provided to protect the blade-root connections and improve the hydrodynamic performance. The material properties of the brackets, the bolts, and the spacer are presented in Table 2.

Table 2. Material properties of brackets and bolts

	Bolts/Bracket/Spacer	(Unit)
E	206000	MPa
G	79230	MPa
ν	0.3	-

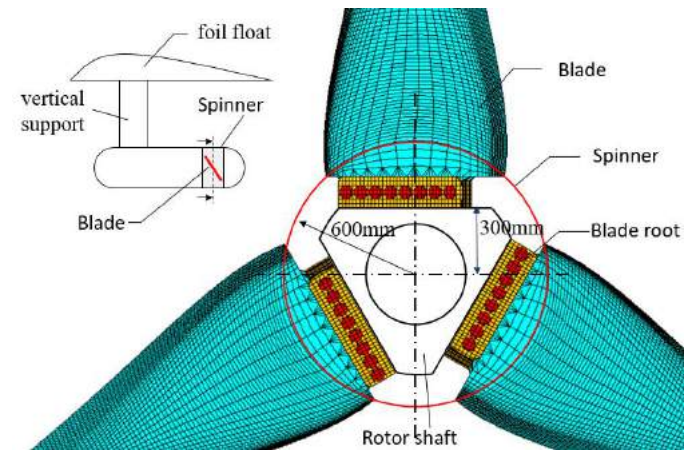


Fig. 5. Blade root connection to the rotor shaft.

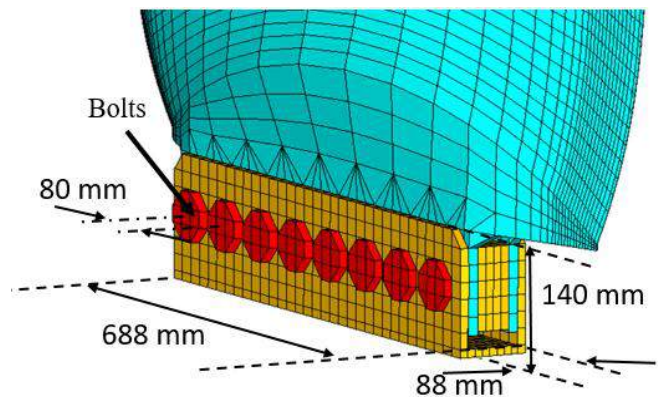


Fig. 6. Detailed view of the bolted bracket connection at the blade root.

MESH DISCRETIZATION

For wind turbines, the skins of the FRP blades are commonly modeled using shell elements for convenience. However, the considered blade geometry is twisted and comprises large variations of thickness, so that a discretization approach of the blade skins using shell elements would not have allowed for an accurate modeling of the blade structure. Fig. 7 shows the comparison of modeling through shell and solid elements. It can be observed, especially at the leading and trailing edges, that the shell elements do not reflect the actual geometry. Therefore, continuum (i.e. solid) shell elements were chosen for a more accurate modeling and because they allow for the assessment of the Tsai-Wu strength criterion. Solid elements were then employed for the representation of the core, bracket, spacer and bolts. In this study, the commercial software Abaqus was used for the structure response analyses. Table 3 lists the element types, the materials and the number of elements employed for each part of the model.

Table 3. FE model element types, materials and number of elements.

	FRP	core	Brackets	8 Bolts
Total number of elements	22543	7617	1338	224
Element shape	Wedge Brick	Wedge Brick	Wedge\Brick	
Element type	C3D6 C3D8	SC6R SC8R	SC6R \ SC8R	

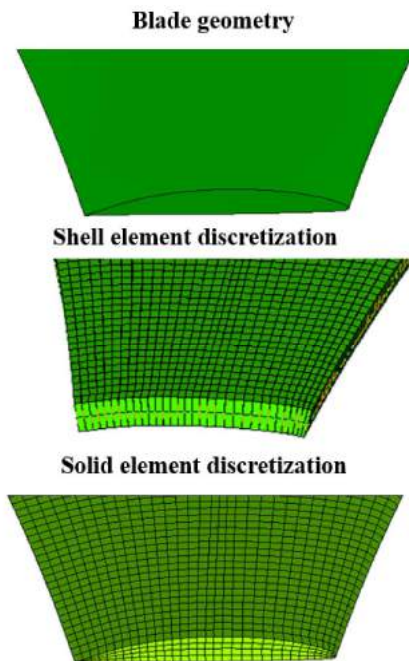


Fig. 7. Comparison of the blade finite element meshing by shell and solid elements.

BOLTED BRACKET ASSEMBLY

The contact between the bolts, the bracket, the spacer and the FRP blade root's skins was reproduced using Abaqus 'surface-to-surface' contact method (Kim, Yoon, and Kang, 2007; Krolo, Grandic, and Bulic, 2016) with a friction coefficient set to 0.4 (see Fig. 8). The eight M20 bolts were preloaded using Abaqus 'Bolt Preload' method, as shown in Fig. 9, to 70% of their tensile capacity for slip-resistance that

corresponds to ~113 kN. Figure 10 shows the distribution of preload pressure on the blade root FRP. An average contact pressure between bolts of 13 MPa can be observed that will not significantly affect the FRP strength. Besides, it is worth noting that the high pressures at the bolt holes' edges (here, ~33 MPa) were disregarded since their square geometry in the FE model could not reproduce correctly the smooth pressure distribution around the real circular holes.

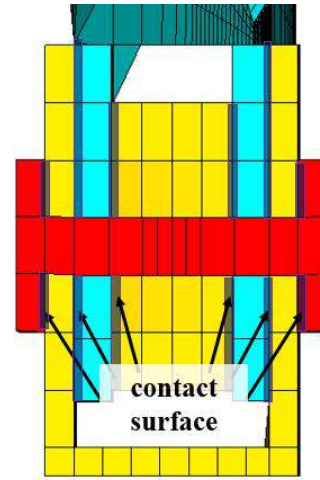


Fig. 8. Contact definition in the bolted bracket assembly.

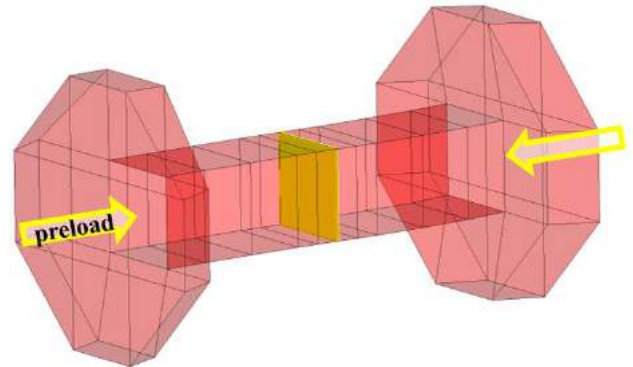


Fig. 9. Bolt preload application at mid-length.

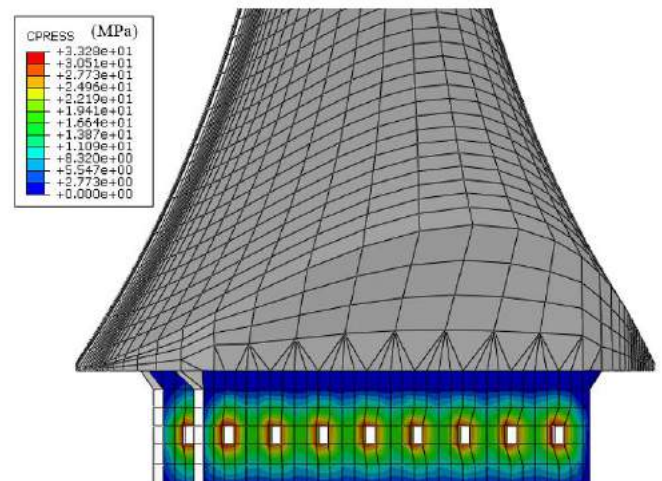


Fig. 10. Distribution of the preload contact pressure on the blade root.

BOUNDARY CONDITIONS

The bottom of the U-profile brackets was assumed rigidly fixed to the rotor shaft. Moreover, the spinner shell was assumed as not providing any support to the blade root connection and was thus omitted from the blade-root modeling. Fig. 11 shows the fixed boundary conditions applied on the bottom of the bracket.

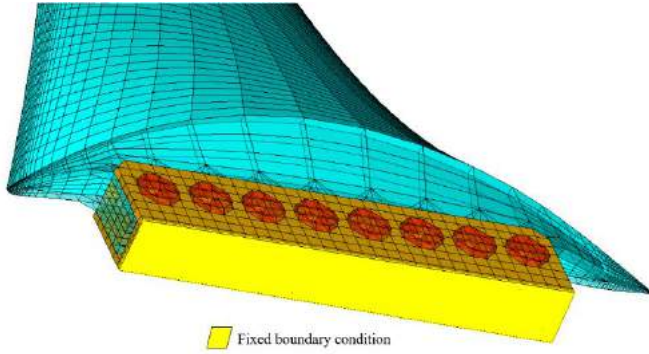


Fig. 11. Fixed bottom of the U-profile brackets.

ULTIMATE STRENGTH ASSESSMENT

Two load cases were considered to evaluate the ultimate strength of the FRP blades. Load case 1 regards the nominal power production and included the 50 m water depth hydrostatic pressure and the hydrodynamic pressure produced by RANS-formulation CFD simulations corresponding to a current velocity of 1.5 m/s and a rotor rotational speed of 0.5 rps (see Fig. 12). The centrifugal force was neglected due to the turbine's low rotational speed.

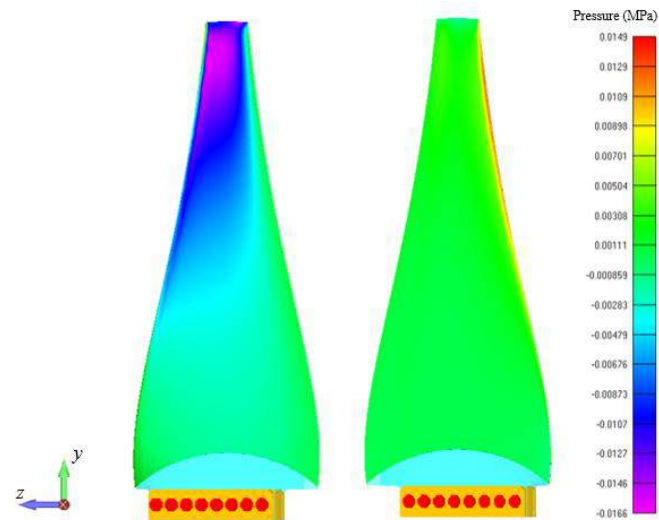


Fig. 12. Pressure distribution on blade for load case 1 (left: suction side, right: pressure side)

Load case 2 was related to an accidental loading condition arising from a collision with drifting debris or marine mammals and it was considered in a 'fail safe' manner, where a quasi-static concentrated force was applied at the blade tip with an increasing amplitude until the failure of the blade, while the blade-root connection was verified against yielding. In this case, 30 accidental loads were applied in the plane normal to the blade length, and the directions of the loads were set every 12° from 12° to 360°, as shown in Fig. 13.

The interaction from multidirectional stress and strain must be considered because the FRP blade skins are compiled of layers of fibres having different orientations. The Tsai-Wu criterion was thus used to evaluate the FRP skin strength. In addition, the fiber stress criteria were also employed to evaluate the fiber strength with regard to the stresses acting along the fibers, those acting perpendicularly to the fibers, and the shear stresses in each layer of the laminate. Finally, the Von Mises stress criterion was used to evaluate the strength of the foam of the blade core and that of the steel bracket at the blade root.

This study adopted the safety factors defined in DNVGL (2015) and BV (2015), as shown in Table 4. The safety factors of DNVGL include the effects of base material, material degradation, production method, temperature, humidity, curing, sandwich constructions, and load categories; whereas BV's safety factors consider the allowable stress, ageing effect of the composites, fabrication process, reproducibility of the fabrication, load carried by the fibers and the core, and type of loads.

Table 4. Safety factors applicable for load case 1 (ultimate limit state) and load case 2* (accidental limit state).

	FRP				CORE	
	M225	DBLT1800/L900				
	$\sigma_{//fiber}$, $\sigma_{\perp fiber}$, τ_{fiber}	$\sigma_{//fiber}$	$\sigma_{\perp fiber}$	τ_{fiber}	σ_1, σ_2	τ_{12}
DNVGL	2.45/2.49*					
BV for fiber stress criteria	3.86	5.02	2.32	3.86	2.75	3.44
BV for Tsai-Wu criteria	3.47	3.47			2.48	

In general, the safety factors defined in BV are more conservative than those in DNVGL.

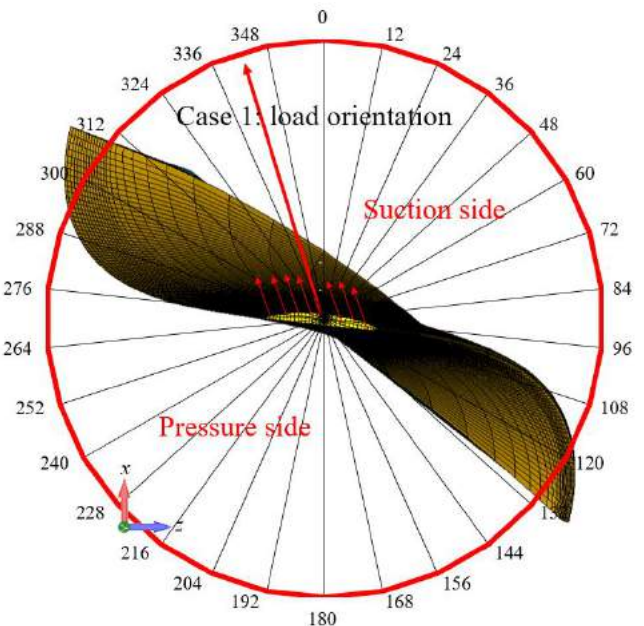


Fig. 13. Orientations of accidental loads at the blade tip

Load case 1: Nominal power production

The loads were applied in two steps. First, the bolt preload was produced to prevent the slippage of the blade root in the bracket. Then,

the hydrostatic and hydrodynamic pressures were applied. The static analysis was carried out through Abaqus considering the geometrical nonlinearities observed at various time-steps.

The obtained blade-tip deflection of 86.7 mm was small compared to blade length (~2.0 m), so that the hydrodynamic performance of the turbine would not be affected. The deformation and Tsai-Wu factor distribution of the FRP blade for load case 1 are shown in Fig. 14 and Fig. 15, respectively.

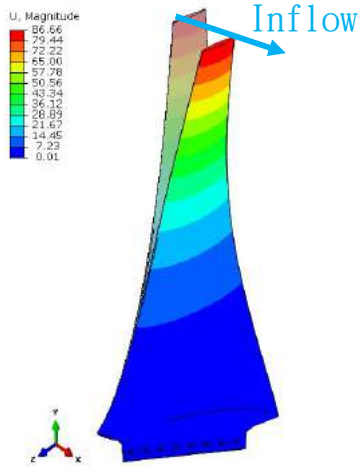


Fig. 14. Deformation of the FRP blade for load case 1

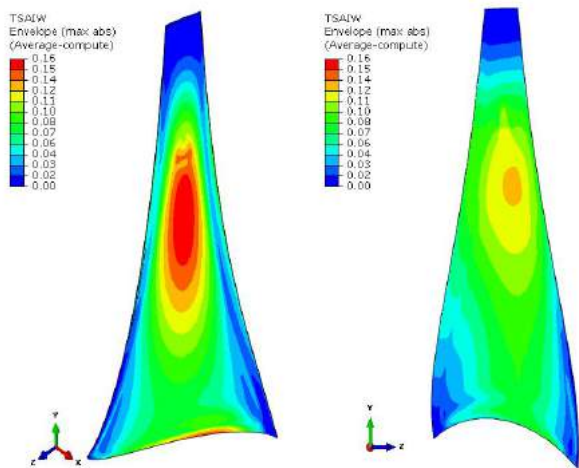


Fig. 15. Tsai-Wu factor distribution on the FRP blade for load case 1 (left : suction side, right : pressure side).

Fig. 15 shows the contour distribution of the largest Tsai-Wu criterion over the 29 layers of FRP on the suction and pressure side of the blade. It can be observed that the highest values were located at mid-length of the blade. Table 5 summarizes the strength verification results in terms of utilization ratio (i.e ratio of working to permissible values). The blade structural strength for load case 1 complied with all the relevant criteria since all utilization ratios were lower than 1.0. The most critical laminates with regard to the strength were located close to the outermost layer. Specifically, it can be observed that ply 27, with a fiber direction of 90° that is perpendicular to the blade bending stress, had utilization ratios of 0.92 and 0.87 according to DNVGL and BV safety factors, respectively. Although this laminate layer's strength was not compromised (i.e. utilization ratio < 1.0), a laminate with 45° fiber

orientation could improve the safety margin while providing some transverse stiffness as ensured by the 90° fiber of the considered ply.

Table 5. Strength verification for load case 1.

	Strength criteria	Working / Permissible		Critical area
		DNVGL	BV	
FRP	$\sigma_{//fiber}$	0.25	0.5	Ply25 DBLT1800 0°
	$\sigma_{\perp fibre}$	0.92	0.87	Ply27 DBLT1800 90°
	τ_{fiber}	0.37	0.58	Ply27 DBLT1800 90°
	Tsai-Wu	0.39	0.56	Ply28 DBLT1800 -45°
Core	VM Stress	0.64	0.64	Core-Tip
	Principal Stress	0.47	0.53	Core-Tip

Load case 2: Abnormal condition

Load case 2 concerns an accidental loading condition arising from a collision with adrift debris or marine mammals and it was considered in a 'fail safe' manner, where a quasi-static concentrated force was applied at the blade tip with an increasing amplitude until the failure of the blade, while the blade-root connection was verified against yielding. This design approach enabled us to ensure that the failure of the blades will occur before compromising the structural integrity of the blade root connection, thereby limiting the cost of blade replacement operations.

In this case, as in load case 1, the loads were applied in two loading steps. After the bolt preload step, the combination of the nominal hydrodynamic pressure and of the blade-tip accidental load were applied. The static analysis was carried out through Abaqus considering the geometrical nonlinearities observed at various time-steps.

For load case 1, the total hydro-static and -dynamic loading on each blade was 5.4 kN with an orientation as illustrated in Fig. 13 (here, 342 deg) and a center of force located at mid-length approximately. The accidental load at the blade-tip was first set to 5.4 kN with 30 different orientations. The blade strength was then evaluated using the Tsai-Wu criterion considering the safety factors provided by DNVGL and BV. The bracket strength was assessed using the Von Mises stress criterion compared to the material yield stress of 315 MPa reduced by a safety factor of 1.1. Fig. 16 shows the most critical results of the strength verification here reported as utilization ratio (i.e. ratio of working to permissible value) in the blade and the bracket for each orientation of accidental loads. It can be observed that, for most of the investigated accidental load orientations, the blade utilization ratio (UR) was larger than that of the bracket and, as such, the blade failure would occur before compromising the strength of the bracket connection. The largest strength difference can be observed for an accidental load at 168° (i.e. almost opposite to hydrodynamic load of case 1) where the blade strength (UR=2.75) was approximately 8.0 times smaller than that at the blade root (UR=0.34) and almost 7.6 times smaller than that of the bracket (UR=0.36). On the other hand, when the accidental loads almost aligned with the hydrodynamic loads, the largest strength difference appeared for an accidental load at 324°, where the blade strength (UR=2.58) was approximately 2.6 times smaller than that at the blade root (UR=0.98) and almost 6.0 times smaller than that of the bracket (UR=0.43). The smallest strength difference can be observed at 96° and 276° for which the blade strength was slightly higher than the bracket yielding strength. However, for those accidental load

orientations that are tangent to the rotor axis, the strength exceedance would be mitigated by the blade rotation.

Fig. 17 shows the location of the maximum Tsai-Wu criterion in the blades for 3 accidental load orientations, namely 0° (i.e. approximately the direction of the resulting force of load case 1), 96° (i.e. approximately perpendicular to the direction of the resulting force of load case 1) and 180° (i.e. approximately opposite to the direction of the resulting force of load case 1). It can be observed that the most critical blade strength results were all located at the mid-length of the blade. The results at the blade root, that here was defined as the region just above the bracket connection (see Fig. 17), were also reported. The highest Von Mises stresses in the bracket all appeared at the base of the vertical frames of the U-profile. Additionally, for accidental loads parallel to the chord line, here $[84^\circ:120^\circ]$ and $[252^\circ:288^\circ]$, the failure area would shift to the trailing and leading edges of the blade. It is worth noting that the highly stressed areas at the bolt hole edges were disregarded in this strength evaluation since their square geometry in the FE model could not reproduce correctly the smooth stress distribution around the real circular holes.

The accidental load investigation was extended to more blade-tip load amplitudes, namely 3.5, 4.5, and 7.0 kN, simulated for the 30 orientations defined in Fig. 13. Fig. 18 shows the ratio of the most critical blade strength utilization ratio to that of the blade root strength (left) and to that of the bracket strength (right), for the four blade-tip loads amplitude examined. It can be observed that the orientations of accidental load that yielded the largest difference of strength between the blade and the bracket remained the same as previously discussed, namely 168° and 324° . In addition, the difference of strength between the blade and the bracket increased quasi-linearly with the amplitude of the accidental loads. Therefore, the geometrical nonlinearities did not influence the results and it can be concluded that any load amplitude will generate the same difference of strength between the blade and the bracket.

Therefore, the large strength difference between the blade and the bracket validated the 'fail safe' design of the bracket connection. However, it is understood that, in the future, further examinations are needed to define more adapted failure criteria of the FRP material than the Tsai-Wu criterion here employed.

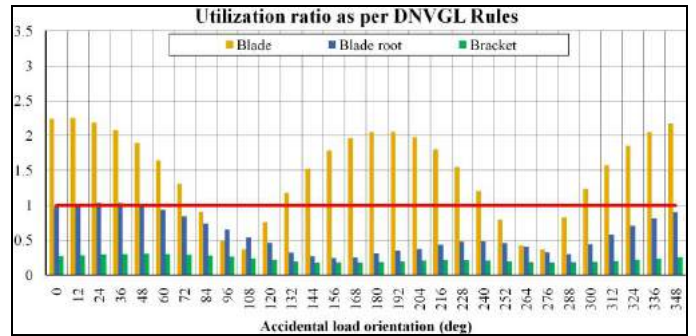
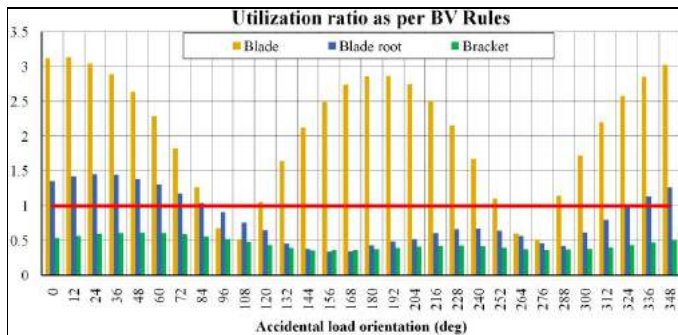


Fig. 16. Strength criteria of blade, root, and bracket by DNV and BV Rules during different loading directions.

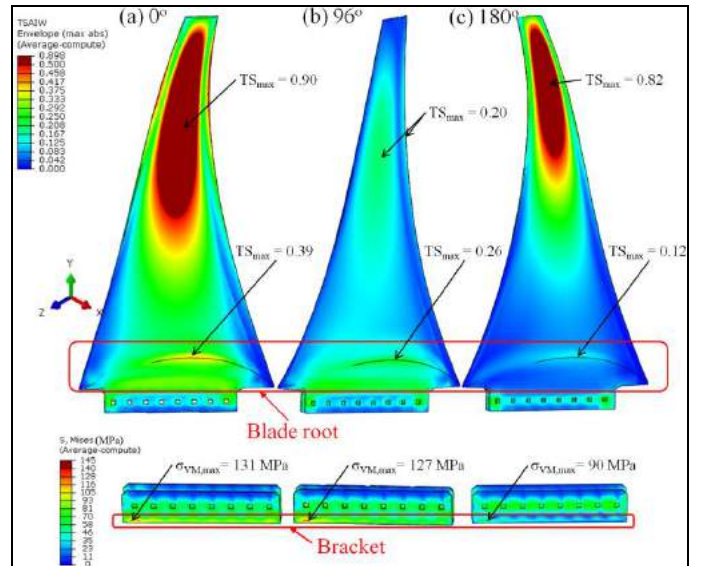


Fig. 17. The location of maximum Tsai-Wu value (red area) for FRP material for 0° , 96° and 180° loading directions.

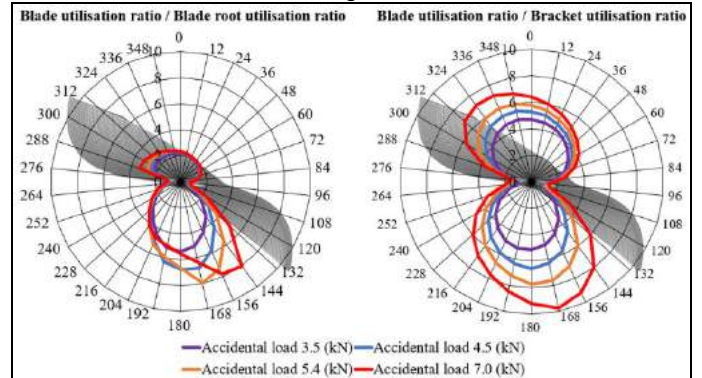


Fig. 18. Comparison of strength criteria under different loading amplitudes.

CONCLUSIONS

This study investigated the ultimate strength of the FKT hydroturbine blade under nominal and accidental loading conditions. Finite element analyses were conducted to evaluate the structural response of the blades, made of fiber reinforced plastic sandwich-structured composite materials, and of the blade-root connection. For the nominal condition, the hydrostatic pressure corresponding to the operational depth and the hydrodynamic pressure, as computed by RANS-formulation CFD for

the average current speed, were applied on the FE model. The results showed that the blade structure complied with all the strength criteria according to BV and DNVGL Rules. The most critical region of the blade with regards to the Tsai-Wu strength criterion appeared to be at mid-length on the suction side. For the accidental loading condition, a collision load acting on the blade-tip was applied, in combination with the nominal load, for various orientations in the plane normal to the blade length to represent the impact of the blade with adrift debris or marine mammals. The accidental loads arising from collision were not considered realistically, but in a 'fail safe' manner to verify that the strength of the root connection made of steel parts was stronger than the blade. This design approach enabled ensuring that the failure of the blades will occur before compromising the structural integrity of the blade root connection, thereby limiting the cost of blade replacement operations. For most of the examined direction of accidental blade-tip loads, the FE results showed a blade strength lower than that of the blade-root connection. The smallest strength difference between the blade and the bracket was found for accidental loads tangent to the rotor. However, for that impact load orientation, it is believed that the rotation of the rotor would mitigate the strength exceedance of the structure. For accidental loads along with and opposite to the current direction, the blade strength was found significantly lower than the bracket connection, and as such the blade failure would preserve the blade-root connection. However, it is understood that, in the future, further examinations are needed to define a more adapted failure criteria of the FRP material than the yielding criteria here employed. Similarly, realistic blade-tip accidental loads could be produced by the collision simulation with rigid debris at constant speed and by

considering the motions of the hydroturbine during such events.

ACKNOWLEDGMENTS

This research project is funded by the Ministry of Science and Technology under National Energy Program, Phase II, Taiwan, R.O.C., MOST 104-3113-E-002-020-CC2.

REFERENCES

- Bureau Veritas (2015). "NI 603 Current and Tidal Turbines"
- Chiu Fang-Ling, Lai Sin-An, Lee Chi-Fang, Tzeng Yu-An, and Hsin Ching-Yeh (2018). "Design and Analysis of the Floating Kuroshio Turbine Blades," *Proc 4th Asian Wave and Tidal Energy Conf*, Taipei, AWTEC2018-491.
- Chiu Forng-Chen, Lin Hsiao-Yu, and Lin Yu-Hsien (2015). "Simulation on the Deployment and Recovery of a Floating Kuroshio Turbine," *National Energy Program-Phase II, 2015*
- DNV-GL (2015). "DNVGL-ST-0164 Tidal turbines"
- Kim Jeong, Yoon Joo-Cheol and Kang Beom-Soo (2007). "Finite element analysis and modeling of structure with bolted joints," *Applied Mathematical Modelling*, 31, 895-911.
- Krolo Paulina, Grandic Davor, and Bulic Mladen (2016). "The Guidelines for Modelling the Preloading Bolts in the Structural Connection Using Finite Element Methods," *Journal of Computational Engineering*, 2016, 8